Perspectives of Scaling up of Severe Plastic Deformation: A Case of High Pressure Torsion Extrusion

Yulia Ivanisenko*

Institute for Nanotechnology, Karlsruhe Institute for Technology, Karlsruhe, 76021 Germany

A demand for cheap and simple methods of processing of nanocrystalline materials attracted attention to metal forming techniques allowing introduction of large strains into metallic materials. Thanks to that a new scientific field, "Materials by severe plastic deformation", had been born and became an important segment of material science. High pressure torsion (HPT) is the most effective SPD method in respect of the microstructure refinement and processing costs. Despite attractive mechanical and physical properties demonstrated by HPT-processed materials, this technique cannot be used in industry due to a limited size of processed samples. To overcome this problem, a plenty of SPD methods, allowing processing of large-scale billets, was developed. However, none of them has found any application in industry, except a few cases, which are rather exceptions that confirm the rule. This overview is an attempt to analyze the reasons why industrial players remain reluctant to use SPD in technological processes. For this purpose, the advantages and drawbacks of the High Pressure Torsion Extrusion method of SPD are regarded.

Keywords: *severe plastic deformation, nanocrystalline and nanostructured materials, mechanical properties, High Pressure Torsion Extrusion, Finite Element Method*

1. Introduction

1.1 Pre-conditions for the scientific research field "Nanomaterials by severe plastic deformation" appearance

The era of nanocrystalline (nc) and nanostructured (ns) materials emerged in the early 80s of the last century with a number of revolutionary works of H. Gleiter,[1–3] where he proposed and demonstrated that nc and ns materials are interesting objects of materials research and have a great potential for structural and functional applications thanks to novel and enhanced mechanical and physical properties. Nanomaterials have a very large volume fraction of interfaces (grain boundaries), and are, therefore, in a metastable state. Due to that processing of nc materials is extremely difficult. Gleiter suggested to use methods of physical vapor deposition for processing of nc materials; in particular, he proposed a method of inert gas condensation (IGC).[2] In this method metals or alloys were evaporated in a vacuum chamber with inert gas atmosphere, typically 100 Pa. Tiny metallic clusters were deposited at a surface of a stainless steel cylinder placed inside the vacuum chamber, subsequently scraped from it, collected and consolidated under high pressure. As-obtained pellets had a uniform nanocrystalline structure with equiaxed grains and a grain size of typically 10–15 nm. Obviously, IGC method is very time consuming, expensive and has a low yield. In facts, a quite limited number of laboratories in the world constructed and exploited such equipment. Deposition of thin nanocrystalline films[4,5] is less complicated and has been used more widely, however resulting microstructures typically have nanocolumnar appearance and possess strong crystallographic texture which makes them less attractive objects for basic research. The above mentioned methods are "bottom-up", as they produce nc samples "atom-by-atom" or "layer by layer".

A strong demand for cheap and easy methods for processing bulk samples with nanocrystalline microstructure suggested the scientists to look in the opposite, "top-down" direction, i.e. to find a way to refine the coarse-grained microstructure of metals and alloys to nano- or submicrometer scale. First of all, mechanical attrition or ball milling (MA/BM) were applied,[6,7] industrial methods which are widely used in various branches like metallurgical, chemical or mining industries to grind substances like metals, chemicals, ores, paints, etc. It appeared that despite laboratory scale high energy ball mills can be effectively used for processing of nanocrystalline powders of various metals and alloys, this approach had obvious drawbacks: powders were contaminated with the material of balls, and should be subsequently consolidated to bulk pellets. Therefore almost simultaneously with the beginning of active use of MA/BM for nc materials processing, it was proposed to subject bulk metallic samples to very large plastic deformation in order to refine their microstructure.[8–10] At first, already existing metal forming techniques, allowing introduction of very high strains into a material, were considered. These techniques were: High Pressure Torsion (HPT, invented by P. Bridgman in the mid of 30s of the last century[11]), Equal Channel Angular Pressing (ECAP, invented by V. Segal in the 70s of the last century[12]), Accumulated Roll Bonding (ARB)[13] and Multiple Forging (MF).[14] The ARB mimics the ancient Chinese forging practice "BAI-LIAN CHENG-GANG", that means "A hundred repetitions of processing (foldings and forgings) makes good steel",[15] and MF is nothing else as the usual forging processing practicing by blacksmiths since the bronze age. In order to use these techniques for the production of nanostructured samples, it was vitally necessary to confirm the formation of ultrafine-grained microstructure, distinct from the cold-worked one. The orientation imaging characterization techniques were in rudimentary stage at that time (end of 80s of the last century), and an unambiguous confirmation that microstructure of materials processed by

*Corresponding author, E-mail: julia.ivanisenko@kit.edu

ECAP and HPT indeed contains predominantly high angle grain boundaries, delivered the experiments of Valiev *et al.*[9] In this work the authors demonstrated that HPT-processed Al–4%Cu–0.5%Zr alloy showed superplastic behavior at relatively low for this alloy temperature of 220°C, which could be realized only thanks to the activation of grain boundary sliding and acceleration of grain boundary diffusion. During 10 years after this publication, the scientific research field "Nanomaterials by severe plastic deformation" has been established, which was documented in a fundamental review paper by Valiev *et al.*[16] that has been cited 6200 times by now. Since that time the number of published investigations on nc and ns materials processed by severe plastic deformation (SPD) started to grow exponentially.[17]

1.2 Material science and engineering in the field of nanomaterials by severe plastic deformation

Almost from the beginning, investigations in the field of nanomaterials, produced by SPD, expanded in two large pathways, basic research and application oriented research. The first one was aimed to understand the materials behavior at intense plastic straining.[18] The mechanisms of grain refinement, influence of processing parameters, driving forces and mechanisms of SPD-driven phase transformations, deformation mechanisms, physical and mechanical properties of SPD-processed materials – these and other issues were studied in dozens of laboratories around the globe. This is not the aim of the present overview paper to describe the findings and discoveries produced during this search, the readers are addressed to a large number of review papers, books and journal special issues, see, for example[19–25] and references therein.

These investigations demonstrated that SPD is a versatile tool for microstructure design, as it allows not only grain refinement down to submicron and even nanoscale range, but also GBs design, variation of phase composition (alloy design) and formation of desirable textures. As already mentioned, the first SPD techniques were HPT, ECAP, MF and ARB. Upon that HPT is the most effective in respect of reachable strain, versatility of materials, grain refinement and processing costs, but size of HPT-samples is rather small. That is why significant efforts were undertaken to invent SPD methods allowing processing of bulk samples. In the last 30 years a number of methods was proposed: Twist Extrusion,[26] Repetitive corrugation and straightening,[27] ECAP-Conform™,[28] KOBO Type Forming,[29] High-pressure tube twisting,[30] Dual Equal Channel Lateral Extrusion (DECLE),[31] High-Pressure Sliding,[32,33] HPT for ring shape samples,[34] Cyclic extrusion-compression,[35] Plastic flow machining,[36] Friction-Assisted Lateral Extrusion,[37] Incremental Feeding High-Pressure Sliding (IF-HPS)[38,39] and some others. Detailed description of SPD scaling up methods can be found in a recent overview paper by Z. Horita *et al.*[40] Now one can realize that despite an obvious demonstration of advantages of SPD-processed materials, not a single SPD method has found a wide application in industry. Up to now there are just two commercial enterprises that use SPD technology: one is the teeth implant company in Czech Republic,[41] and the second one is the company producing sputter targets for electronic industry in USA.[42] Problems related with challenges of commercialization of SPD techniques are discussed in a recent review.[43] In most cases, the main issue for materials processing in industry is the expenditure of time, since it is directly related to the performance of a process. Furthermore, the processing time is even more important in such cases where phase transformations or deformation annealing take place during the processing. Many SPD techniques have a common limitation as they require a repetition of deformation passes with breaks in-between. Moreover, some surface treatment between the passes might be necessary. Therefore these methods cannot be smoothly included in a technological processing chain (may be with an exception of ECAP-Conform™).[28] To overcome this disadvantage a method reproducing the stress-strain conditions at HPT in a rod-shape sample had been proposed.[44] The method was called High Pressure Torsion Extrusion (HPTE).

2. A Continuous SPD Method of High Pressure Torsion Extrusion

All technical details of the method were published elsewhere.[45,46] In short, a rod-shape specimen is deformed by the punch (moving with the velocity v) as well as by the containers (one of them rotates with the velocity ω) (Fig. 1) in such a way that the entire length of a specimen is torsionally deformed, as a specimen gradually passes through the shear zone. In order to constrain torsional deformation within a thin surface layer of a specimen, and to prevent slippage of the specimen, the channel design was modified to include special holding elements (Fig. 1).

2.1 Strain distribution in the billet at HPTE

For the estimation of the strain e accumulated by the specimen, a simple equation was proposed in Ref. 46):

$$e = 4\,ln\frac{D2}{D1} + 2\,ln\frac{D1}{D3} + \frac{\omega \cdot R}{\sqrt{3}\cdot v}\frac{D2}{D1} \qquad (1)$$

Where D1, D2 and D3 are the diameters of the HPTE die channels (Fig. 1), v is translational velocity and ω is rotational velocity. In the above equation it is assumed that strains due to expansion-extrusion and torsion are additive.

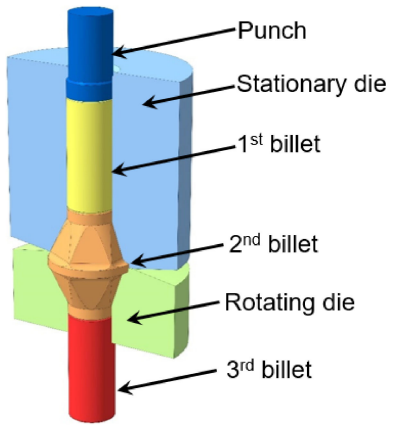

Fig. 1 Schematic drawing of the HPTE process with three billets inside the die.[45] With permission of Elsevier.

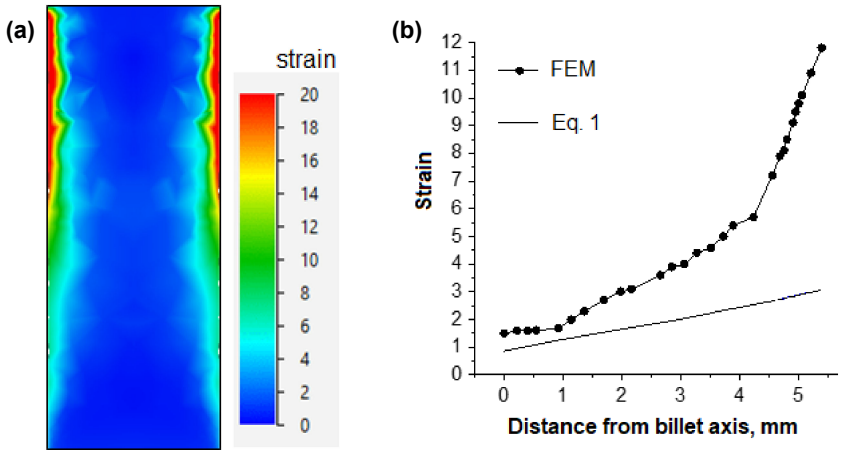

Fig. 2 (a) Strain distribution after HPTE $v6\omega1$ at 25°C of copper in the longitudinal cross section of the billet. (b) Accumulated strain distribution in transversal cross section at the half of billet height, calculated by FEM and by eq. (1) for $v6\omega1$ HPTE regime performed at 25°C.

The first two terms in the eq. (1) refer to a strain achieved in a round bar after conventional extrusion. The third term corresponds to the upper bound strain estimate for the HPT process. Modeling of the HPTE process using Finite Element Method (FEM)[45] had shown that eq. (1) describes the strain distribution not accurately, as the complex shape of the die channels (Fig. 1) and friction conditions are not taken into account. For example, Fig. 2(a) shows FEM calculated strain distributions in a Cu billet deformed by HPTE at room temperature with translational velocity $v = 6$ and rotational velocities $\omega = 1$, and Fig. 2(b) shows the variations of the accumulated strain from the center of the billet to its edge in the middle of its height calculated by eq. (1) and by FEM. One can see a deviation between the strain distributions calculated by eq. (1) and by FEM. This deviation is especially large close to the billet edge which is related to strong friction between the billet and the die surfaces. Therefore FEM simulations describe the strain distribution in the sample more realistically in comparison with that calculated by eq. (1).

2.2 Microstructure refinement at HPTE

Accumulated strain at HPTE increases from the billet axis to the billet edge in a similar way as at conventional HPT. Figure 3 shows the inverse pole figure maps of the microstructures formed in commercially pure copper close to the billet axis, at the middle of radius and at the edge after HPTE via the $v1\omega1$ regime at room temperature[46] and at 100°C.[47]

One can see that the microstructure formed at both temperatures in the billet close to its axis is very inhomogeneous, and EBSD analysis confirmed a presence of a large fraction of LAB. Whereas the grain structure in the mid-radius and edge areas was rather uniform, with almost equiaxed grains and a high fraction of HABs. The mean grain size was larger in the sample processed at 100°C than that in the sample processed at RT (0.7…0.8 μm and 0.4 μm, respectively).

Similarity of the grain size in billet regions experienced different strain at HPTE (eq. (1), Fig. 2) indicates that the saturation of the grain size refinement was reached, which is typical for other SPD methods.[19]

It should be emphasized, that microstructures resulting from the HPTE processing are rather complex, which is a common feature of structures formed after other SPD-techniques. In particular, Automated Crystal Orientation Mapping (ACOM) TEM provided additional microstructural details of the HPTE-processed copper.[47] Whereas a conventional bright field image (Fig. 4(a)) is not very informative, an orientation map shown in Fig. 4(b) allows to recognize individual grains, high- and low angle grain boundaries and nano-twins. One should note that new grains formed after HPTE can be simultaneously bounded by high angle and low angle boundaries. Furthermore, spatial distribution of geometrically necessary dislocations (GND), shown in Fig. 4(c), clearly demonstrates that the GND density differed significantly in neighboring (sub)grains, which means that both LABs and special (twin) boundaries provided effective barriers for the dislocation slip and they should be taken into account in the analysis of possible strengthening factors, in particular Hall–Petch strengthening.

By now HPTE was successfully used for processing commercially pure Al and 6101 Al alloy, Mg and ZK30, ZK60 Mg alloys. For example, the influence of various HPTE regimes on the microstructure of pure Al was analyzed in Ref. 48). Figure 5 shows the OIM maps of the microstructures formed in Al after $v7\omega1$, $v1\omega1$ and $v1\omega3$ HPTE regimes at the middle of the billet radius. By increasing the accumulated strain, the grain size decreased while the HAGB fraction increased, and most of these changes occurred up to the strain value of ~5. Between the strains of ~5 to ~20, only a moderate decrease in grain size from ~1 μm to 0.7 μm was observed, and a saturation in microstructures was reached.

The study[48] clearly demonstrated that HPTE provides an efficient grain refinement in Al comparable to that of ECAP and HPT processes. In the processed sample by HPTE regime $v1\omega1$, the mean grain size at the equivalent strain of ~20 was about ~0.7 μm; whereas further increase in strain via the HPTE regime $v1\omega3$ did not change the grain size. Therefore, grain size refinement saturation is observed for HPTE processing of Al as well. The same mean grain size was obtained in 1050 Al alloy after eight passes of ECAP[49,50] and

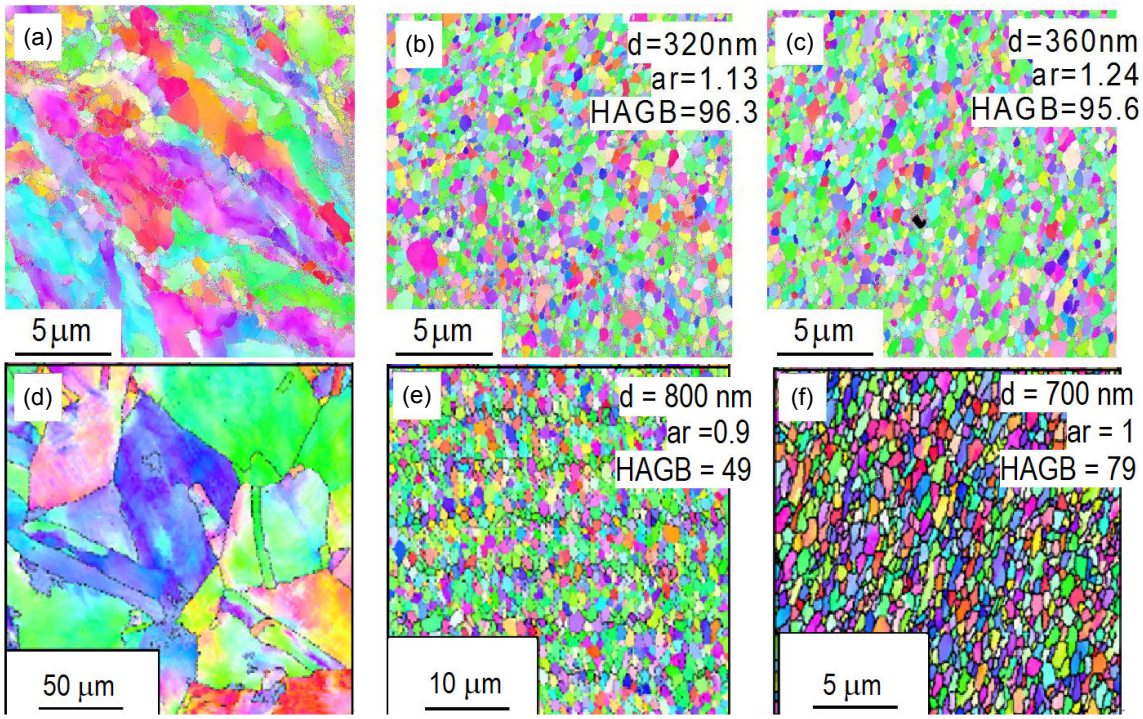

Fig. 3 Orientation maps (inverse pole figure maps) of Cu specimens processed by using HPTE via the $v1\omega1$ regime at room temperature (a)–(c) and at 100°C (d)–(f) in areas close to: (a), (d) – the billets axis; (b), (e) – middle radius, (c), (f) – edge. Colouring corresponds to the projection of normal direction (ND) in the inverse pole figure. Characteristic microstructural values such as mean grain size (d), aspect ratio (ar) and fraction (%) of high angle grain boundaries (HAGB) are also indicated. Figures (a)–(c) reprinted from Ref. 47) with permission.

HPT.[51,52] It should be noticed, however, that ECAP requires about 10 passes to accumulate necessary amount of strain in materials, whereas HPTE provides this strain level only within one pass, thereby simplifying and accelerating the processing of high-strength, bulk aluminum.

2.3 Mechanical properties of materials processed by HPTE

Both microhardness and tensile strength of Cu processed by HPTE are significantly increased in comparison with these values in annealed state. Upon that uniform elongation is reduced to a few percent, but total elongation remains rather large, practically the same as that of the annealed sample (Fig. 6). This is in agreement with "Strength-ductility paradox" proclaimed for some SPD–processed materials in Ref. 53). Table 1 summarizes the mechanical properties of Cu, processed by HPTE at room temperature in comparison with the respective values after conventional HPT and ECAP with several passes.[54] One can see that mechanical properties of Cu after HPTE are higher than these after several passes of ECAP, and comparable with these after HPT.

Therefore it can be concluded that HPTE appears to be feasible for fabricating metallic samples with similarly small grain size and enhanced mechanical properties as obtained by HPT, but in a bulk form.

2.4 HPTE processing of architectured materials

HPTE can be also used for processing of hybrid or architectured samples.[55] Composite materials are widely used for structural applications; they contain soft matrix with embedded reinforcements that have simple shapes (particles, straight rods, meshes, etc.). Application of HPTE to a rod sample with inserted straight hardening wires leads to a refinement of the matrix microstructure and transforms the shape of wires from straight one to helical (Fig. 7(a)). Such architectures resemble the morphology of natural tissues having high fracture toughness (bones, shells, …),[56,57] and can be used for parts operating in conditions of shock loading, for example.

2.5 Combination of HPTE with Conform™

Laboratory-scale HPTE machine described in Refs. 46), 47) is not a really continuous process, as the length of the billet is limited by the length of the punch. After processing of one billet, punch should be removed and a new billet should be placed in the die. This prevents the industrial use of the method. In order to be able to apply HPTE for billets with much larger length, it was proposed to combine it with the Conform™ process.[58] This idea was realized virtually with the help of FEM modelling.

The principle of the Conform™-HPTE process is shown schematically in Fig. 8. The long billet is fed into the Conform-wheel and can be continuously extruded through all deformation chambers, upon that the Conform-wheel provides the extrusion force. During the process, the billet fills all deformation chambers, which provides backpressure for the subsequent HPTE process. As a model material for calculations AA 6201 aluminum alloy billet with a diameter of 10 mm was used.

In order to satisfy the common conditions of industrial processing of aluminum alloys, following regimes were used for FEM simulations: Conform-wheel rotation rate was 1, 2

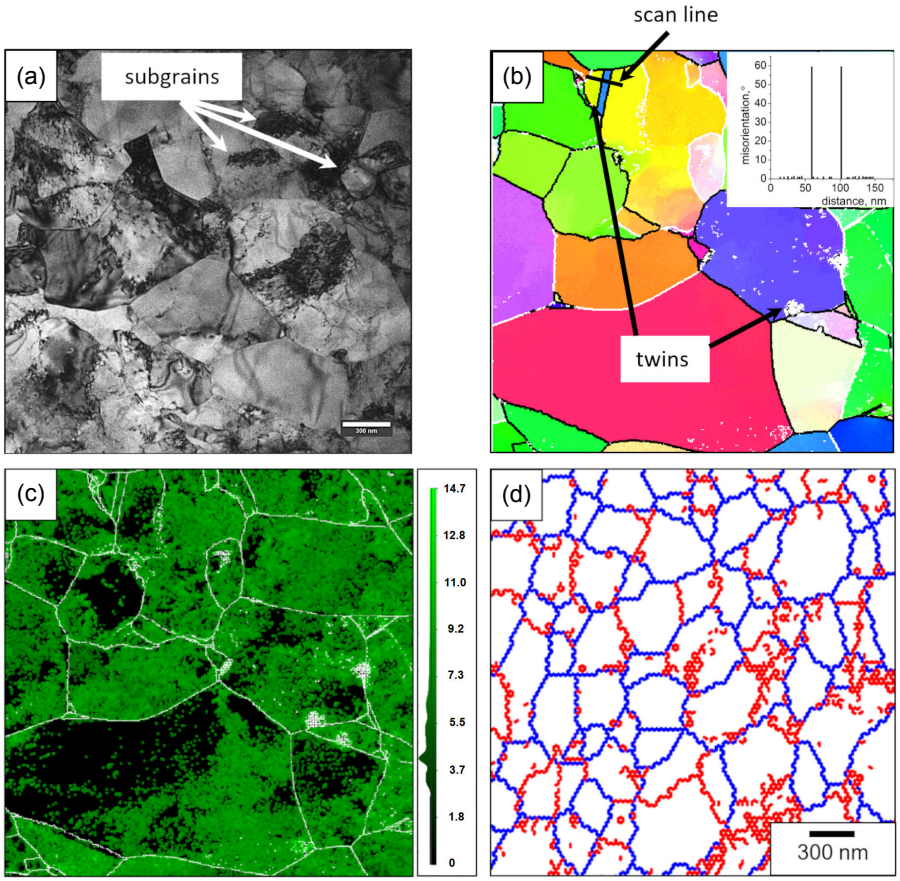

Fig. 4 Microstructure of the HPTE-processed Cu in the mid-radius area of the longitudinal section. (a) TEM BF image; (b) ACOM TEM OIM map in which LABs ($3° < \Theta < 15°$ are highlighted with white lines) and HABs ($\Theta > 15°$ are highlighted with black lines). Inset shows the orientation variation along the indicated scan line; (c) GND distribution map from ACOM TEM (all GBs are marked with white lines). Inset at the right hand side shows color code map, each value is $\times 10^9$ m^{-2}; and (d) EBSD OIM GBs network (LABs marked with red lines, HABs marked with blue lines). All the images are at the same scale. Reprinted from Ref. 47) with permission of MDPI.

and 3 rpm, corresponding Conform outlet translational velocity (in the 5-5 section in Fig. 8) was 575, 1150 and 1725 mm/min, HPTE rotational velocity (ωHPTE) was rather high, from 58 to 518 rpm. FEM calculations were performed to analyze stress, strain and strain rate distributions in the billet volume and variation of the billet temperature during processing. For example, the temperature contour during Conform™-HPTE process with Conform wheel velocity of 1 rpm and HPTE rotation velocity of 58 rpm is shown in Fig. 9(a), and temperature variation along the deformation zone for all modelled regimes are shown in Fig. 9(b). After final Conform reduction, the temperatures at the Conform die exit (section 5–5 in Fig. 8) are 290, 315 and 330°C for Conform velocities varying from 1 to 3 rpm, respectively, such temperature rises are quite normal for industrial Conform production of Al alloys (~300–450°C, depending on the Conform-wheel velocity). Therefore there is no need to pre-heat the billet before the HPTE deformation, which takes full advantage of the characteristic feature of Conform™ process.[59,60)]

The material temperature increases further during the subsequent HPTE deformation, upon that the maximum temperature is about 460°C at Conform-wheel velocity of 3 rpm and HPTE velocity of 518 rpm (Fig. 9(b)). One should note that temperatures in the range 300–460°C are high enough to activate a grain growth in Al alloys, however it may require some time. The translational velocities at simulated HPTE-Conform™ process were rather high – from 0.6 to 1.7 m/min, that means that the temperature exposure of the sample would be rather short. On the other hand, HPTE processing at such temperatures might result in larger saturated grain size in comparison with that after room temperature treatment. Therefore it is necessary to build the set up and to perform real experiments in order to decide which additional equipment (e.g. cooling system) would be necessary to maintain ultrafine-grained structure.

Figure 10 shows the equivalent plastic strain distribution during the Conform™-HPTE process. The strain achieved after Conform is about 2.9 (plane 5–5). Then the subsequent HPTE deformation further introduces large amount of strain in the billet. After one single deformation pass of the Conform™-HPTE process, the mid-radius strain at the die exit is about 8.3 (Fig. 10(a)). However the strain is not homogeneous and is gradiently distributed, strain at the edge is larger than that in the center (Fig. 10(b)).

These simulations showed that the proposed combination of Conform™ and HPTE is fully feasible and can be realized at a commercial enterprise.

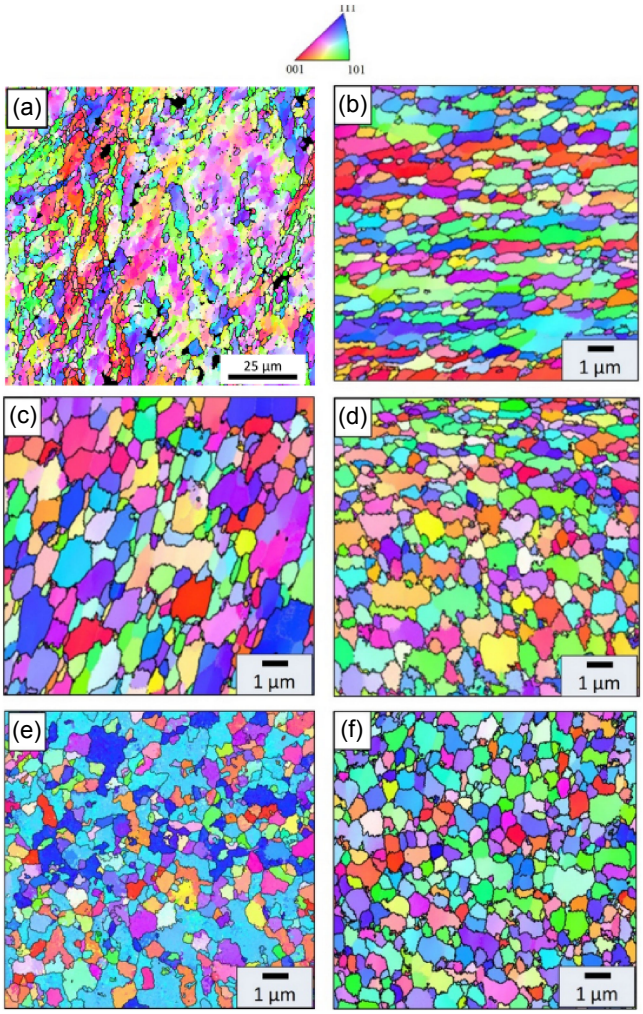

Fig. 5 Orientation maps of Al taken at the mid-radius zones (a), (c), (e) and at the edge zones (b), (d), (f) of HPTE samples under the regimes of $v7\omega1$ (a), (b), $v1\omega1$ (c), (d), $v1\omega3$ (e), (f). Reprinted from Ref. 48) with permission of Elsevier.

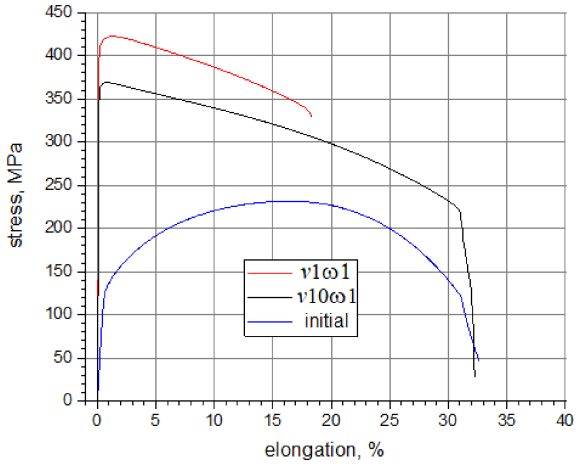

Fig. 6 Tensile stress-elongation curves of Cu processed by HPTE at room temperature with translation rates of 1 mm/min and 10 and rotation rate of 1 rpm in comparison with tensile curve of coarse grained Cu.

Table 1 Vickers hardness (HV), yield strength (YS), ultimate strength (UTS) and elongation to failure (δ) of Cu after HPTE, HPT and ECAP.

Process parameters	HV	YS, MPa	UTS, MPa	δ, %	Source
soft rod ASTM		100	220	>5.0	ASTM B49-17
HPTE $v10\omega1$ RT	110	360	370	37	47)
HPTE $v1\omega1$ RT	125	410	420	32	47)
ECAP 3 passes	41	382	404	2.1	
ECAP 18 passes	120	358	415	3.6	
HPT ½ turn	133	474	512	2.0	54)
HPT 10 turns	127	444	487	4.0	

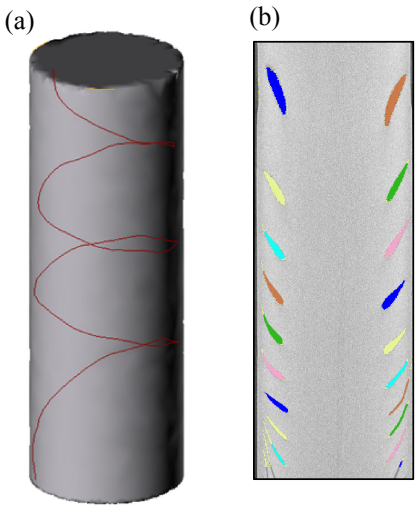

Fig. 7 (a) FEM simulated 3D image of the initially straight marker line after HPTE processing. (b) X-ray tomography images of the aluminum wires in copper billets after HPTE $v6w1$ at 100° in longitudinal cross section.

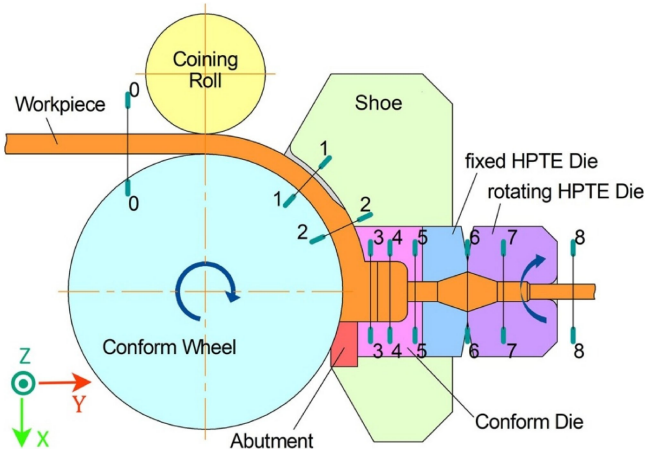

Fig. 8 Schematic diagram of the Conform™-HPTE process. Reprinted from Ref. 58) with permission of Elsevier.

3. Concluding Remarks

To summarize, the continuous SPD method of high pressure torsion extrusion has following advantages:

1. Possibility to process billets with UFG microstructure;
2. Large strain is accumulated during one pass;
3. No additional equipment for creating of back pressure in the die channel is necessary;

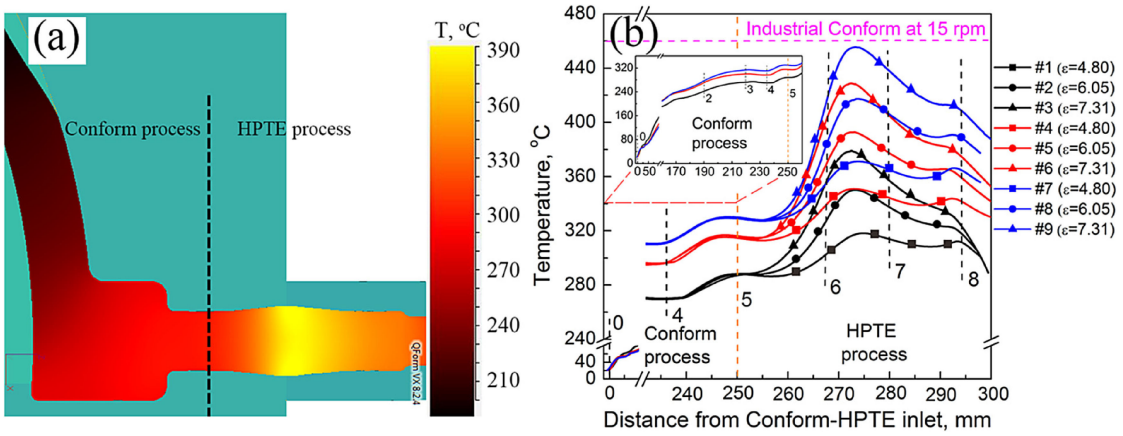

Fig. 9 (a) Temperature distribution during Conform™-HPTE process with Conform wheel velocity of 1 rpm and HPTE rotation velocity of 173 rpm; (b) temperature variation along the deformation zone for all regimes (#1…9) studied in Ref. 53). The numbers near the dashed lines indicate the planes shown in Fig. 8. Reprinted from Ref. 58) with permission of Elsevier.

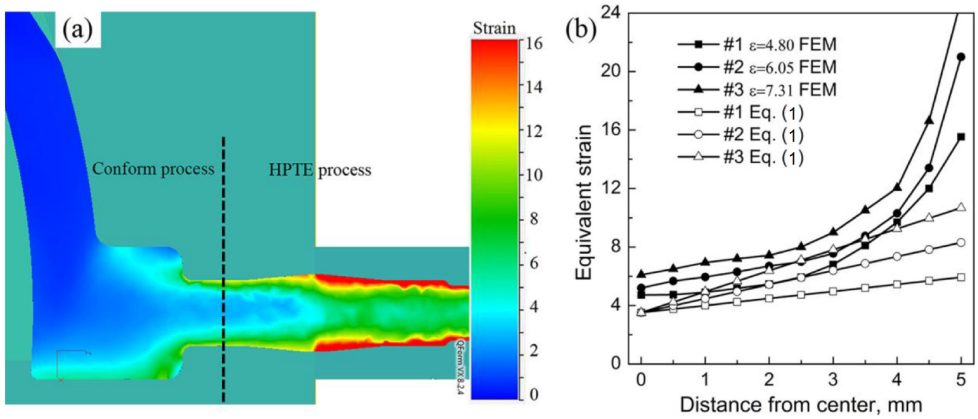

Fig. 10 (a) Equivalent plastic strain distribution during Conform™-HPTE process with Conform wheel velocity of 1 rpm and HPTE rotation velocity of 173 rpm, and (b) equivalent strain in dependence on the distance from the billet axis calculated using FEM and eq. (1) after a single Conform-HPTE deformation pass. # numbers indicate different regimes regarded in Ref. 58). Reprinted from Ref. 58) with permission of Elsevier.

4. Varying the processing parameters either homogenous or gradient UFG microstructure can be produced;
5. The method can be used for processing of hybrid materials with helical architecture of reinforcements;
6. In combination with Conform™ process rods of practically unlimited length can be produced.

Despite these obvious advantages, the HPTE method still had not found any application in industry, in a similar way as it had happened with other SPD techniques. We should state that industrial players remain reluctant to the attempts of NanoSPD community to commercialize severe plastic deformation. Along with general conservativism of business stakeholders, the following disadvantages, usually not discussed openly, but quite important for commercial enterprises are:

1. Low production rate;
2. Low tools endurance;
3. Reproducibility in case of mass-production is in doubt;
4. Processing is expensive.

In facts, SPD is still a hand working process similar to ancient blacksmiths work, despite the presence of heavy machines and computer control. In this respect, the application area might be in the fields of medical and luxury products, as well as in small-scale techniques: drones, robots, sensors, etc. Therefore the attempts to convince industrial partners should be continued.

However it would be wrong to end this overview on a sour note. As it had been emphasized in the beginning, severe plastic deformation is a fantastic tool for materials science basic research, and investigations of materials behavior at combined action of very high pressures and strains can contribute to understanding of physical mechanisms governing and driving metastable phase transformations, microstructure refinement, interplay between various hardening mechanisms and many other phenomena and processes. These efforts should be further supported by more profound use of computational methods of material science, and creation of digital twins of various microstructural processes is expected.

REFERENCES

1) H. Gleiter: Mater. Sci. Eng. **52** (1982) 91–131.
2) R. Birringer, U. Herr and H. Gleiter: Trans. JIM **27**(Suppl.) (1986) 43–47.
3) H. Gleiter: Prog. Mater. Sci. **33** (1989) 223–315.
4) A. Sherman: *Chemical Vapour Deposition for Microelectronics*, (Park

Ridge-Noyes, New Jersey, 1987).
5) K.L. Choy: Prog. Mater. Sci. **48** (2003) 57–170.
6) C.C. Koch: Nanostruct. Mater. **2** (1993) 109–129.
7) C. Suryanarayana: *Mechanical Alloying and Milling*, (Marcel Dekker, New York, 2004) pp. 336–342.
8) N.A. Smirnova, V.I. Levit, V.P. Pilugin, R.I. Kuznezov, L.S. Davidova and V.A. Sazonova: Phys. Met. Metallogr. **6** (1986) 1170.
9) R.Z. Valiev, O.A. Kaibyshev, R.I. Kuznetsov, R.Sh. Musalimiv and N.K. Tzenev: Sov. Phys. Dokl. **33** (1988) 626–627.
10) N.H. Ahmadeev, R.Z. Valiev, V.I. Kopylov and R.R. Mulyukov: Russ. Metall. **5** (1992) 96–101.
11) P.W. Bridgman: Phys. Rev. **48** (1935) 825–847.
12) V.M. Segal, V.I. Reznikov, A.E. Drobyshevskiy and V.I. Kopylov: Russ. Metall. **1** (1981) 99–105.
13) Y. Saito, N. Tsuji, H. Utsunomiya, T. Sakai and R.G. Hong: Scr. Mater. **39** (1998) 1221–1227.
14) O.R. Valiahmetov, R.M. Galeyev and G.A. Salishchev: Fiz. Met. Metalloved. **10** (1990) 204–206.
15) J.T. Wang: Mater. Sci. Forum **503–504** (2006) 363–370.
16) R.Z. Valiev, R.K. Islamgaliev and I.V. Alexandrov: Prog. Mater. Sci. **45** (2000) 103–189.
17) Z. Horita and K. Edalati: Mater. Trans. **61** (2020) 2241–2247.
18) Y. Estrin and A. Vinogradov: Acta Mater. **61** (2013) 782–817.
19) R. Pippan, S. Scheriau, A. Taylor, M. Hafok, A. Hohenwarter and A. Bachmaier: Annu. Rev. Mater. Res. **40** (2010) 319–343.
20) R.Z. Valiev, Y. Estrin, Z. Horita, T.G. Langdon, M.J. Zehetbauer and Y. Zhu: JOM **68** (2016) 1216–1226.
21) A. Hohenwarter and R. Pippan: Philos. Trans. R. Soc. London Ser. A **373** (2015) 20140366.
22) M. Kawasaki, B. Ahn, P. Kumar, J. Jang and T.G. Langdon: Adv. Eng. Mater. **19** (2017) 1600578.
23) K. Edalati and Z. Horita: Mater. Trans. **60** (2019) 1103.
24) Bulk-Nanostructured Materials. Special Issue Adv. Eng. Mater. **17** (2015) 1699–1875.
25) K. Edalati *et al.*: Mater. Res. Lett. **10** (2022) 163–256.
26) Y. Beigelzimer, V. Varyukhin, S. Synkov and D. Orlov: FIZTV (Fizika and Tekhnika Vysokikh Davlenii) **9** (1999) 109–110.
27) Y.T. Zhu, H. Jiang, J. Huang and T.C. Lowe: Metall. Mater. Trans. A **32** (2001) 1559–1562.
28) G.J. Raab, R.Z. Valiev, T.C. Lowe and Y.T. Zhu: Mater. Sci. Eng. A **382** (2004) 30–34.
29) W. Bochniak and A. Korbel: J. Mater. Process. Technol. **134** (2003) 120–134.
30) L.S. Toth, M. Arzaghi, J.J. Fundenberger, B. Beausir, O. Bouaziz and R. Arruffat-Massion: Scr. Mater. **60** (2009) 175–177.
31) B. Talebanpour and R. Ebrahimi: Mater. Des. **30** (2009) 1484–1489.
32) T. Fujioka and Z. Horita: Mater. Trans. **50** (2009) 930–933.
33) Y. Takizawa, T. Masuda, K. Fujimitsu, T. Kajita, K. Watanabe, M. Yumoto, Y. Otagiri and Z. Horita: Metall. Mater. Trans. A **47** (2016) 4669–4681.
34) K. Edalati and Z. Horita: Mater. Trans. **50** (2009) 92–95.
35) N. Pardis, B. Talebanpour, R. Ebrahimi and S. Zomorodian: Mater. Sci. Eng. A **528** (2011) 7537–7540.
36) V.Q. Vu, Y. Beygelzimer, L.S. Toth, J.-J. Fundenberger, R. Kulagin and C. Chen: Mater. Charact. **138** (2018) 208–214.
37) V.Q. Vu, L.S. Toth, Y. Beygelzimer and Y. Zhao: Materials **14** (2021) 2465.
38) Y. Takizawa, K. Sumikawa, K. Watanabe, T. Masuda, M. Yumoto, Y. Kanai, Y. Otagiri and Z. Horita: Metall. Mater. Trans. A **49** (2018) 1830–1840.
39) T. Komatsu, T. Masuda, Y. Tang, I.F. Mohamed, M. Yumoto, Y. Takizawa and Z. Horita: Mater. Trans. **64** (2023) 436–442.
40) Z. Horita, Y. Tang, T. Masuda and Y. Takizawa: Mater. Trans. **61** (2020) 1177–1190.
41) http://www.timplant.cz/en/
42) S. Ferrasse, V.M. Segal, F. Alford, S. Strothers, J. Kardokus, S. Grabmeier and J. Evans: *Severe Plastic Deformation: Toward Bulk Production of Nanostructured Materials*, ed. by B.S. Altan, (Nova Science Publishing, NY, 2005) pp. 585–601.
43) T.C. Lowe, R.Z. Valiev, X. Li and B.R. Ewing: MRS Bull. **46** (2021) 265–272.
44) V.T. Fedorov, Yu. Ivanisenko, B. Baretzky and H. Hahn: Vorrichtung und Verfahren zur Umformung von Bauteilen aus Metallwerkstoffen. German patent DE 10 2013 213 072.4, European patent EP 2 821 156 B1.
45) D. Nugmanov, R. Kulagin, O. Perroud, M. Mail, H. Hahn and Y. Ivanisenko: J. Mater. Process. Technol. **315** (2023) 117932.
46) Yu. Ivanisenko, R. Kulagin, V. Fedorov, A. Mazilkin, T. Scherer, B. Baretzky and H. Hahn: Mater. Sci. Eng. A **664** (2016) 247–256.
47) D. Nugmanov, A. Mazilkin, H. Hahn and Y. Ivanisenko: Metals **9** (2019) 1081.
48) B. Omranpour, Y. Ivanisenko, R. Kulagin, L. Kommel, E. Garcia Sanchez, D. Nugmanov, T. Scherer, A. Heczel and J. Gubicza: Mater. Sci. Eng. A **762** (2019) 138074.
49) E.A. El-Danaf, M.S. Soliman, A.A. Almajid and M.M. El-Rayes: Mater. Sci. Eng. A **458** (2007) 226–234.
50) Y. Cao, L. He, Y. Zhou, P. Wang and J. Cui: Mater. Sci. Eng. A **674** (2016) 193–202.
51) M. Naderi, M. Peterlechner, S.V. Divinski and G. Wilde: Mater. Sci. Eng. A **708** (2017) 171–180.
52) Y. Ito and Z. Horita: Mater. Sci. Eng. A **503** (2009) 32–36.
53) R.Z. Valiev, I.V. Alexandrov, Y.T. Zhu and T.C. Lowe: J. Mater. Res. **17** (2002) 5–8.
54) M.Y. Alawadhi, S. Sabbaghianrad, Y. Huang and T.G. Langdon: J. Mater. Res. Technol. **6** (2017) 369–377.
55) Y. Estrin, Y. Beygelzimer and R. Kulagin: Adv. Eng. Mater. **21** (2019) 1900487.
56) U.G.K. Wegst, H. Bai, E. Saiz, A.P. Tomsia and R.O. Ritchie: Nat. Mater. **14** (2015) 23.
57) L. Li, J.C. Weaver and C. Ortiz: Nat. Commun. **6** (2015) 6216.
58) J.M. Hu, R. Kulagin, Yu. Ivanisenko, B. Baretzky and H. Zhang: J. Manuf. Process. **55** (2020) 373–380.
59) X. Kong, H. Zhang and X. Ji: Mater. Sci. Eng. A **612** (2014) 131–139.
60) Y. Zhao, B. Song, J. Pei, C. Jia, B. Li and G. Linlin: J. Mater. Process. Technol. **213** (2013) 1855–1863.